Filomat 40:8 (2026), 3015–3042
https://doi.org/10.2298/FIL2608015A

Published by Faculty of Sciences and Mathematics,
University of Niš, Serbia
Available at: http://www.pmf.ni.ac.rs/filomat

An efficient numerical solution of multi-term fractional pantograph differential equations via generalized Bell functions

İbrahim Avcı[a,*], Şuayip Yüzbaşı[b]

[a] *Department of Basic Sciences and Humanities, Faculty of Arts and Sciences, Cyprus International University, Nicosia, via Mersin 10, Türkiye*
[b] *Department of Mathematics, Faculty of Science, Bartın University, Bartın, TR 07058, Türkiye*

Abstract. In this study, we propose an efficient numerical method for multi-term fractional pantograph differential equations (FPDEs) with Caputo derivatives, covering both linear and nonlinear models. The method builds an operational matrix of fractional integration in a generalized Bell basis and reduces the FPDE to a compact algebraic system in the Bell coefficients. Nonlinear terms (powers/products, including delayed interactions) are treated by projection-based (pseudo-operational) matrices within the same framework. Solving the resulting system determines the coefficients and yields the approximate solution in explicit Bell form. We provide convergence and error analyses, and numerical experiments demonstrate high accuracy—often near machine precision—with modest truncation and consistently low CPU time on standard hardware. Relative to results reported in the literature, the proposed scheme attains comparable or better accuracy at reduced computational cost, highlighting its practicality for multi-term FPDEs with delays.

1. Introduction

Fractional calculus stands as a pivotal branch in mathematical analysis, representing a generalization of differentiation and integration to non-integer orders. This field, characterized by its roots in the speculations of Gottfried Leibniz (1695) and Leonhard Euler (1730), has evolved continuously, now encompassing various definitions of fractional operators present in the literature. Notable examples include Riemann-Liouville, Caputo, Atangana-Baleanu, and Caputo-Fabrizio operators. While fractional calculus boasts a history dating back centuries, it has experienced a remarkable surge in growth, emerging as a dynamic and rapidly evolving domain of mathematics, as evidenced by recent developments in the field. For a comprehensive overview of the historical progression of fractional calculus, interested readers can refer to [12, 19, 24].

A fractional differential equation (FDE) is a generalized class of differential equations that is integer order derivative operators replaced by non-integer order operators. Fractional derivative operators involved in FDEs are highly efficient mathematical tools for modeling and defining phenomena in social and natural sciences. The powerful properties of fractional operators, especially so-called the memory effect, motivated

2020 *Mathematics Subject Classification*. Primary 26A33; Secondary 34A08, 34K40.
Keywords. numerical analysis, fractional differential equations, Caputo derivative, generalized Bell functions, operational matrix.
Received: 24 October 2024; Revised: 28 September 2025; Accepted: 17 January 2026
Communicated by Marko Petković
* Corresponding author: İbrahim Avcı
Email addresses: ibrahima@ciu.edu.tr (İbrahim Avcı), suayipyuzbasi@bartin.edu.tr (Şuayip Yüzbaşı)
ORCID iDs: https://orcid.org/0000-0003-0986-2195 (İbrahim Avcı), https://orcid.org/0000-0002-5838-7063 (Şuayip Yüzbaşı)

many researchers for describing mathematical systems with fractional models. Consequently crucial roles of such operators can be seen in various real world problems such as finance [14], mathematical biology [20], chemistry [3], electromagnetics [13], physics [25], signals processing [22], economics [30], fluid mechanics [17], control [27], and many more.

Pantograph differential equations represent a distinctive class of delay differential equations (DDEs) characterized by a proportional delay argument, particularly prevalent in the realm of electrodynamics. These equations capture phenomena where a system's response depends on its past states in a proportional manner. The fractional pantograph differential equation (FPDE) is an extension of the pantograph differential equation to non-integer orders, introducing fractional calculus into the framework. This generalization allows for a more nuanced description of systems exhibiting memory effects and complex dynamics. In general, since finding an analytical solution to FPDE is difficult, developing efficient numerical methods for such equations becomes an important focus for researchers. Consequently, a considerable amount of research papers has been published to find highly accurate approximate solutions to FPDEs. Some of the developed numerical methods for solving FPDE existing in the literature can be mentioned as the Spectral Galerkin Method [5], Generalized Lucas Polynomials Method [31], Haar Wavelet Method [2], Fractional Taylor Operational Matrix of Fractional Integration Method [8], Legendre Wavelet Method [32], Vieta–Fibonacci Wavelets Method [6], Chebyschev Wavelets Method [16] and so forth. In our specific study, we target the solution of a multi-term version of the fractional pantograph differential equation. In this context, 'multi-term' denotes differential equations that involve more than one fractional derivative operator. This extension accommodates systems with intricate dependencies on multiple past states, broadening the applicability of the model to various real-world scenarios. By solving the multi-term fractional pantograph differential equation, our aim is to provide a comprehensive and efficient numerical approach to tackle complex dynamic systems exhibiting fractional-order behavior.

In 1938, Lanczos [18] introduced the so-called Spectral methods, which have gained a great deal of interest in recent years for solving various types of problems [1, 4, 9, 28, 34]. The most important advantages that make these methods attractive are that they are easy to apply and provide high-efficiency results, especially if the problem has a smooth solution, they provide "exponential rate of convergence" accuracy. Basically, spectral methods are formed by describing the solution of a problem as a linear combination of a set of spectral basis functions which are infinitely differentiable, and determining the coefficients to satisfy the solution of the given problem. The collocation, Tau, and Galerkin are known as three types of spectral methods. In this study, we use the spectral collocation method that seeks the solutions of FPDEs using generalized Bell polynomials.

A general class of the pantograph-type differential equations, which may include both linear and nonlinear forms, is given as:

$$u'(x) = f\left(x, u(x), u'(x), u(px), u'(px)\right), \ x \in [0, T], \tag{1}$$

where f is a continuous function and p denote a proportional delay with $0 < p < 1$.

In this study, motivated by the strong modeling features of fractional derivative operators, we propose a new technique based on generalized Bell polynomials and focus on approximate solutions of general FPDEs, that is a generalization of pantograph-type differential equation (1) to the non-integer order, defined in the following form:

$$D^{\beta}u(x) = f\left(x, u(x), D^{\mu}u(x), u(px), D^{\delta}u(px)\right), \ x \in [0, T], \tag{2}$$

with initial conditions

$$u^{(n)}(0) = \varphi_n, \ n = \{0, 1, ..., \lceil\beta\rceil - 1\}, \tag{3}$$

and

$$u(x) = \omega(x), \ x < 0.$$

where D^{β}, D^{μ}, D^{δ} denotes the Caputo fractional derivative operators to the orders β, μ, δ, respectively, with $\beta \geq \mu$ and $\delta > 0$, and ω is a known continuous function.

Our paper develops an efficient numerical method for a broad class of multi-term FPDEs with Caputo derivatives, covering both linear and nonlinear models. The key idea is to construct an operational matrix of fractional integration in a generalized Bell basis, which converts the FPDE into a compact algebraic system in the Bell coefficients; nonlinear products (including delayed interactions) are handled by projection-based matrices within the same framework. Solving this system yields the coefficients and, hence, an explicit Bell-basis approximation. The method is supported by convergence and error analyses and by illustrative examples, which show high accuracy with modest truncation and consistently low CPU time. Overall, using generalized Bell polynomials provides a stable, accurate, and versatile tool for FPDEs with delays, offering strong computational efficiency without sacrificing reliability.

The manuscript is organized as follows. Section 2 collects essential definitions and preliminaries from fractional calculus. Section 3 develops the generalized Bell framework, including the operational matrix of fractional integration and the projection-based matrices for nonlinear terms and proportional delay. Section 4 presents the numerical scheme for multi-term fractional pantograph equations, covering both linear and nonlinear cases. Section 5 provides convergence and error analyses. Section 6 reports seven illustrative examples that demonstrate the accuracy and efficiency of the method. Finally, Section 7 concludes and outlines directions for future work.

2. Preliminaries and fundamental definitions

In this part, we give some necessary definitions and preliminary facts of fractional calculus. Besides, we give the representation of the generalized Bell polynomials and function approximation based on them.

Definition 2.1. *[12] The Riemann–Liouville (R–L) fractional integral to order β of the integrable function $u(x)$ is defined as*

$$J^{\beta}u(x) = \begin{cases} \dfrac{1}{\Gamma(\beta)} \displaystyle\int_0^t (x-v)^{\mu-1} u(v)\,\mathrm{d}v, & \beta > 0 \\ u(x), & \beta = 0 \end{cases} \tag{4}$$

When the R–L fractional integral operator utilized to a power function, we get:

$$J^{\beta}(x)^{\rho} = \frac{\Gamma(\rho+1)}{\Gamma(\rho+\beta+1)}(x)^{\rho+\beta},\ \beta \geq 0,\ \rho > -1.$$

The semigroup property of the operator is defined as:

$$J^{\mu}J^{\beta}u(x) = J^{\beta}J^{\mu}u(x),\ \mu,\beta > 0.$$

The R–L fractional integral operator is linear, that is

$$J^{\beta}(k_1u_1(x) + k_2u_2(x)) = k_1J^{\beta}u_1(x) + k_2J^{\beta}u_2(x),$$

for any two functions u_1,u_2 and constants k_1,k_2.

Definition 2.2. *[12] The Caputo derivative of fractional order β for the function $u(x)$ is given as*

$$D^{\beta}u(x) = J^{q-\beta}\left(\frac{\mathrm{d}^q}{\mathrm{d}x^q}u(x)\right),\ q-1 < \beta \leq q,\ q \in \mathbb{N}. \tag{5}$$

If $v-1 \leq \beta \leq v$, $v \in \mathbb{N}$, then we have the following important relation between the R–L fractional integral and Caputo fractional derivative:

$$J^{\beta}(D^{\beta}u(x)) = u(x) - \sum_{r=0}^{v-1} u^{(r)}(0)\frac{x^r}{r!}.$$

Definition 2.3. *[10] The Bell polynomials can be defined in power form as following*

$$B_m(x) = \sum_{r=0}^{m} C(m,r)x^r$$

where $C(m,r)$ for $m \in \mathbb{N}$ denotes the Stirling number of the second kind which is defined by

$$C(m,r) = \frac{1}{r!}\sum_{j=0}^{r}(-1)^j\binom{r}{j}(r-j)^m.$$

Let

$$\mathbf{B}_M(x) = [B_0(x), B_1(x), ..., B_M(x)]^T.$$

By using the power form expansion of the Bell polynomials, we define

$$\mathbf{B}_M(x) = \mathbf{C}_M\mathbf{V}_M(x), \tag{6}$$

where

$$\mathbf{V}_M(x) = [1, x, x^2, ..., x^M]^T$$

and,

$$\mathbf{C}_M = \begin{pmatrix} C(0,0) & 0 & \cdots & 0 \\ C(1,0) & C(1,1) & \cdots & 0 \\ \vdots & \vdots & \ddots & \vdots \\ C(M,0) & C(M,1) & \cdots & C(M,M) \end{pmatrix}$$

Definition 2.4. *[33] The generalized Bell polynomials can be represented by*

$$B_m^{\gamma}(x) = \sum_{r=0}^{m}\sum_{j=0}^{r}\frac{(-1)^j}{r!}\binom{r}{j}(r-j)^m x^{r\gamma},$$

where $x \in [0,1]$ and $m \in \mathbb{N}_0$. In what follows we take $\gamma > 0$; choosing $\gamma = 1$ reduces the basis to the classical case.

The first few generalized Bell polynomials are given by:

$$B_0^{\gamma}(x) = 1$$
$$B_1^{\gamma}(x) = x^{\gamma}$$
$$B_2^{\gamma}(x) = x^{\gamma} + x^{2\gamma}$$
$$B_3^{\gamma}(x) = x^{\gamma} + 3x^{2\gamma} + x^{3\gamma}$$
$$B_4^{\gamma}(x) = x^{\gamma} + 7x^{2\gamma} + 6x^{3\gamma} + x^{4\gamma}$$
$$B_5^{\gamma}(x) = x^{\gamma} + 15x^{2\gamma} + 25x^{3\gamma} + 10x^{4\gamma} + x^{5\gamma}$$

Therefore, by using the generalized Bell polynomials, the equation (6) can be rewritten as

$$\mathbf{B}_{M,\gamma}(x) = \mathbf{C}_M\mathbf{V}_{M,\gamma}(x) \tag{7}$$

where $\mathbf{B}_{M,\gamma}(x)$ is the vector of generalized Bell polynomials given by

$$\mathbf{B}_{M,\gamma}(x) = [B_0^{\gamma}(x), B_1^{\gamma}(x), ..., B_M^{\gamma}(x)]^T \tag{8}$$

and the vector $\mathbf{V}_{M,\gamma}(x)$ is defined by

$$\mathbf{V}_{M,\gamma}(x) = [1, x^{\gamma}, x^{2\gamma}, ..., x^{M\gamma}]^T. \tag{9}$$

2.1. Function approximation

Consider the vector of generalized Bell polynomials

$$\mathbf{B}_{M,\gamma}(x) = [B_0^\gamma(x), B_1^\gamma(x), ..., B_M^\gamma(x)]^T$$

and let $\mathbf{B}_{M,\gamma}(x) \subset H$ where $H = L^2[0,1]$ also, suppose that $S = span\{B_0^\gamma(x), B_1^\gamma(x), ..., B_M^\gamma(x)\}$. Since S is a finite dimensional vector subspace of H, for any $u \in H$, u has a unique best approximation $u_M \in S$, that is

$$\forall \hat{u} \in S, \ \|u - u_*\| \leq \|u - \hat{u}\|.$$

Since $u_M \in S$, there exist unique coefficients k_i for $i = 0, 1, ...M$ such that

$$u(x) \simeq u_M(x) = \sum_{i=0}^{M} k_i B_i^\gamma(x) = \mathbf{K}^T \mathbf{B}_{M,\gamma}(x), \tag{10}$$

where $\mathbf{B}_{M,\gamma}(x)$ is the generalized Bell vector defined in (9) and $\mathbf{K}$ is the vector of unknown unique coefficients given by

$$\mathbf{K}^T = [k_0, k_1, ..., k_M].$$

The vector $K = [k_0, \ldots, k_M]^T$ collects the unique coefficients of the approximation $u_M \in S := \text{span}\{B_0^\gamma, \ldots, B_M^\gamma\}$ in (10). If a reference function u is known, these coefficients are the L^2-projection on $[0,1]$:

$$G\,K = g, \qquad G_{ij} = \langle B_i^\gamma, B_j^\gamma \rangle_{L^2(0,1)}, \quad g_i = \langle u, B_i^\gamma \rangle_{L^2(0,1)}.$$

In the present problem u is unknown; thus K is determined by enforcing the governing equation. Specifically, we substitute (10) into the integral form of the FPDE (Section 4) and collocate at M+1 nodes on $[0, T]$. This yields a square algebraic system $F(K) = 0$: it is linear ($AK = b$) for linear FPDEs and nonlinear for general FPDEs, in which case we solve it by a Newton–type iteration. Initial conditions are imposed in the same system (through the integral form), and the proportional delay and nonlinear terms are handled via the delay and product operational matrices introduced in Section 3. The uniqueness of K follows from the linear independence of $\{B_i^\gamma\}_{i=0}^M$ and the nonsingularity of the resulting collocation matrix for distinct nodes.

Unless stated otherwise, all problems are posed on $[0, T]$ with $T > 0$. The generalized Bell basis is defined on the reference interval $[0,1]$: $B_{M,\gamma}(s) = [B_0^\gamma(s), \ldots, B_M^\gamma(s)]^T$ for $s \in [0,1]$. For $x \in [0, T]$ we use the scaled basis $\widehat{B}_{M,\gamma}(x) := B_{M,\gamma}(x/T)$ and approximate $u(x) \simeq K^T \widehat{B}_{M,\gamma}(x)$. If a problem is posed on a general interval $[a, b]$, we set $x = a + (b - a)s$ with $s \in [0,1]$ and apply the same construction.

The proportional delay parameter satisfies $0 < p < 1$, hence $px \in [0, T]$ for $x \in [0, T]$, and delayed evaluations are $\widehat{B}_{M,\gamma}(px) = B_{M,\gamma}((px)/T)$. We take $\gamma > 0$ so that the monomial terms $s^{\gamma n}$ are single-valued on $[0,1]$. Note that only u on $[0, T]$ is expanded; the history $\omega(x)$ for $x < 0$ enters as given data and is not expanded in the Bell basis.

3. Operational matrices in the generalized Bell basis

Throughout this section the operational matrices are constructed for the monomial vector $V_{M,\gamma}(x)$ defined in (9).

The Riemann–Liouville fractional integral of order β acts componentwise as

$$J^\beta V_{M,\gamma}(x) = x^\beta D_\beta \, V_{M,\gamma}(x), \qquad D_\beta := \text{diag}\left(\frac{\Gamma(\gamma i + 1)}{\Gamma(\gamma i + \beta + 1)}\right)_{i=0}^{M}.$$

Using the relation (7) between the generalized Bell vector and $V_{M,\gamma}$,

$$B_{M,\gamma}(x) = C_M \, V_{M,\gamma}(x),$$

the corresponding operator on the generalized Bell basis is obtained by a change of basis:

$$J^{\beta}B_{M,\gamma}(x) = C_M J^{\beta} V_{M,\gamma}(x) = x^{\beta}\Big(C_M D_{\beta} C_M^{-1}\Big)B_{M,\gamma}(x) \;\equiv\; P_{(x,\beta)}\, B_{M,\gamma}(x).$$

Consequently, for any expansion $u_M(x) = K^T B_{M,\gamma}(x)$ we have $J^{\beta}u_M(x) = K^T P_{(x,\beta)} B_{M,\gamma}(x)$. In the implementation we act on $V_{M,\gamma}$ and carry C_M explicitly, so computing C_M^{-1} is not required.

By utilizing the operator Riemann–Liouville fractional integral to the order β for the vector $V_{M,\gamma}(x)$, we get

$$J^{\beta}(V_{M,\gamma}(x)) = \left[\frac{1}{\Gamma(\beta+1)}x^{\beta}, \quad \frac{\Gamma(\gamma+1)}{\Gamma(\gamma+\beta+1)}x^{\gamma+\beta}, \quad \cdots, \quad \frac{\Gamma(M\gamma+1)}{\Gamma(M\gamma+\beta+1)}x^{M\gamma+\beta}\right]^T,$$

which can be rewritten as

$$J^{\beta}(V_{M,\gamma}(x)) = x^{\beta} D_{\beta} V_{M,\gamma}(x), \tag{11}$$

where

$$D_{\beta} = \operatorname{diag}\left[\frac{1}{\Gamma(\beta+1)}, \frac{\Gamma(\gamma+1)}{\Gamma(\gamma+\beta+1)}, \frac{\Gamma(2\gamma+1)}{\Gamma(2\gamma+\beta+1)}, \ldots, \frac{\Gamma(M\gamma+1)}{\Gamma(M\gamma+\beta+1)}\right]$$

represents the operational matrix of fractional integration.

Assume that $\Phi_{(x,\beta)} = x^{\beta} D_{\beta}$, then the operational matrix of fractional integration for the generalized Bell polynomials can be defined as

$$P_{(x,\beta)} = \operatorname{diag}\left(\Phi_{(x,\beta)}, \Phi_{(x,\beta)}, \ldots, \Phi_{(x,\beta)}\right). \tag{12}$$

Therefore, equation (11) can be rewritten as

$$J^{\beta}(V_{M,\gamma}(x)) = P_{(x,\beta)} V_{M,\gamma}(x). \tag{13}$$

We use operational matrix for exact operator actions on the chosen basis—in particular, D_{β} and $P_{(x,\beta)}$ in (12)–(13) (and the proportional delay) are operational, since $J^{\beta}V_{M,\gamma}(x) = x^{\beta}D_{\beta}V_{M,\gamma}(x)$ and $V_{M,\gamma}(px) = \operatorname{diag}(p^{\gamma n})V_{M,\gamma}(x)$ hold identically. When an operator/nonlinearity does not map the basis into itself, we use a pseudo-operational matrix, obtained by collocation onto the truncated Bell space.

For nonlinear FPDEs, terms such as $u^2(x)$, $u^3(x)$, or $u(x)u(px)$ must also be expressed in the generalized Bell basis. Suppose that the approximate solution is represented as

$$u(x) \simeq u_M(x) = K^T B_{M,\gamma}(x),$$

where $B_{M,\gamma}(x) = \left[B_0^{\gamma}(x), B_1^{\gamma}(x), \ldots, B_M^{\gamma}(x)\right]^T$ is the generalized Bell vector, and $K = [k_0, k_1, \ldots, k_M]^T$ is the coefficient vector.

Then, a nonlinear term of the form $[u(x)]^2$ can be written as

$$[u(x)]^2 \simeq \Big(K^T B_{M,\gamma}(x)\Big)\Big(K^T B_{M,\gamma}(x)\Big).$$

This product can be re-expressed in the Bell basis using a pseudo-operational product matrix Q (obtained by projection), such that

$$[u(x)]^2 \simeq K^T Q B_{M,\gamma}(x). \tag{3.4}$$

where Q is obtained by projecting the quadratic products of basis functions $B_i^{\gamma}(x)B_j^{\gamma}(x)$ back into the Bell basis.

Similarly, higher-order nonlinearities (e.g., $u^p(x)$ with integer $p \geq 2$) can be expressed by recursively applying the product operational matrix:

$$[u(x)]^p \simeq K^T Q^{(p)} B_{M,\gamma}(x), \tag{3.5}$$

where $Q^{(p)}$ denotes the corresponding p-th order product matrix.

For mixed nonlinearities involving proportional delays, such as $u(x)u(px)$, we expand

$$u(px) \simeq K^T B_{M,\gamma}(px),$$

and then project the product $u(x) \cdot u(px)$ onto the generalized Bell basis:

$$u(x)u(px) \simeq K^T Q^{(px)} B_{M,\gamma}(x), \tag{3.6}$$

where $Q^{(px)}$ is the cross-product operational matrix corresponding to multiplication of $B_{M,\gamma}(x)$ and $B_{M,\gamma}(px)$.

4. Numerical implementation

In this section, we present the numerical implementation of the proposed method, founded on the generalized Bell operational matrix of fractional integration. This framework is designed to solve the multi-term fractional pantograph differential equation as specified in (2), which may include both linear and nonlinear terms.

In the initial phase, the problem expressed in (2) is reformulated in the equivalent integral form by applying the Riemann–Liouville fractional integral of order β and incorporating the initial conditions. This yields

$$u(x) - \sum_{n=0}^{\lceil\beta\rceil-1} \frac{\varphi_n}{n!} x^n = J^\beta\Big(\mathcal{F}[u(x), D^\mu u(x), u(px), D^\delta u(px), f(x)]\Big), \tag{14}$$

where $\mathcal{F}[\cdot]$ denotes the general operator on $u(x)$ and its fractional derivatives.

Next, approximating $u(x)$ by the generalized Bell expansion (10), we obtain

$$K^T B_{M,\gamma}(x) - \sum_{n=0}^{\lceil\beta\rceil-1} \frac{\varphi_n}{n!} x^n = J^\beta\Big(\mathcal{F}[K^T B_{M,\gamma}(x), K^T B_{M,\gamma}(px), f(x)]\Big). \tag{15}$$

By substituting the generalized Bell operational matrix of fractional integration and invoking the nonlinear extension discussed in Section 3, the nonlinear terms in $\mathcal{F}[\cdot]$ are projected onto the Bell basis using the product or cross-product operational matrices Q, $Q^{(p)}$, and $Q^{(px)}$. Thus, (15) reduces to

$$K^T C_M V_{M,\gamma}(x) - \sum_{n=0}^{\lceil\beta\rceil-1} \frac{\varphi_n}{n!} x^n = K^T\Big[C_M P_{(x,\beta)} V_{M,\gamma}(x) \; + \; C_M Q^{(*)} V_{M,\gamma}(x)\Big] + J^\beta f(x), \tag{16}$$

where $Q^{(*)}$ denotes the appropriate nonlinear operational matrix corresponding to the nonlinear structure of $\mathcal{F}$.

Finally, we collocate on Chebyshev–Lobatto nodes,

$$x_i = \frac{T}{2}\Big(1 - \cos\frac{\pi i}{M}\Big), \qquad i = 0, 1, \ldots, M,$$

which provides good endpoint resolution and stable conditioning. This yields a system of $M+1$ algebraic equations in the Bell coefficients K. For linear models the system is linear in K; for nonlinear models it is

nonlinear in K and is solved iteratively. Once K is determined, the approximate solution $u_*(x)$ is recovered from the expansion (2.7).

Nonlinear terms are evaluated on a 3/2 oversampled grid and projected back to the Bell space via column-pivoted QR. Linear systems $AK = b$ are solved with MATLAB's direct solver `A\b`; least-squares projections use pivoted QR. The nonlinear system $F(K) = 0$ is solved with lsqnonlin using a complex-step Jacobian.

For choosing the Bell parameter γ, we match the basis to the leading local behaviour of the solution. Let the right–hand side near $x = 0$ behave like x^q; then for a Caputo derivative of order α the solution behaves like $u(x) \sim x^r$ with $r = \alpha + q$. We set an initial choice $\gamma_0 = r/n$ with a small $n \in \{1, 2\}$, and, if needed, refine γ by a short grid search around γ_0 (e.g., $[\gamma_0 - 0.1, \gamma_0 + 0.1]$) and select the value that minimizes the max–norm error.

5. Convergence and error analysis

In this section of the study, we delve into the convergence and error analysis of the approximate solution obtained through our proposed method. Additionally, we introduce a methodology for establishing an error estimation function tailored to the present technique.

5.1. Error bound for the approximation

Assume that $u(x)$ and $u_M(x) = \mathbf{K}^T\mathbf{B}_{M,\gamma}(x)$ be the exact and approximate solution of the given problem (14) with degree γM. Further, we assume that $u_M^s(x) = \widetilde{\mathbf{K}}^T V_{M,\gamma}(x)$ denotes the generalized Maclaurin series expansion [21] of $u(x)$ with the degree γM. So, the actual error of the approximate solution $u_M^s(x)$ is bounded as

$$\begin{aligned} \|u(x) - u_M(x)\|_\infty &\leq \frac{T^{\gamma(M+1)}}{\Gamma(\gamma(M+1)+1)} \left\|u^{(\gamma(M+1))}(cx)\right\| \\ &+ k_{M,\gamma}\left(\left\|\widetilde{\mathbf{K}}^T\right\|_\infty + \left\|\mathbf{K}^T\right\|_\infty \|\mathbf{C}_M\|_\infty\right) \end{aligned} \tag{17}$$

since the vectors $\mathbf{B}_{M,\gamma}(x)$ and $\mathbf{V}_{M,\gamma}(x)$ are defined in (8) and (9) respectively where $0 \leq x \leq T$, $k_{M,\gamma} = \max\{T^{M\gamma}, 1\}$ and $\Delta\mathbf{K}^T = \mathbf{K}^T - \widetilde{\mathbf{K}}^T$.

5.2. Convergence analysis

The convergence state of the approximate solution $u_M(x) = \mathbf{K}^T\mathbf{B}_{M,\gamma}(x)$ with the assumption that the maximum error in $0 \leq x \leq T$ in fact equals the upper error bound (17) in Theorem 1 is defined by

$$\Delta\widetilde{\mathbf{K}}^T + \|\mathbf{K}_{M+1}\|_\infty \Delta\mathbf{K}^T < \frac{T^{\gamma(M+1)}}{k_{M,\gamma}\Gamma(\gamma(M+1)+1)} u^{(\gamma(M+1))}(0), \tag{18}$$

since $\mathbf{K}^T$ is the coefficient vector for the approximate solution $u_M(x)$, $\widetilde{\mathbf{K}}^T$ denotes the coefficient vector in the generalized Maclaurin polynomial of $u(x)$ with degree $(M\gamma)$, $k_{M,\gamma} = \max\{T^{M\gamma}, 1\}$ and $\Delta\widetilde{\mathbf{K}}^T = \left\|\widetilde{\mathbf{K}}_{M+1}^T\right\|_\infty - \left\|\widetilde{\mathbf{K}}_M^T\right\|_\infty$.

5.3. Error estimation

Let $u(x)$ and $u_M(x)$ be the exact and approximate solutions of the problem (14) respectively. Then,

$$D^\beta u(x) - u(x) - D^\mu u(x) - u(px) + D^\delta u(px) - f(x) = 0, \tag{19}$$

and

$$D^\beta u_M(x) - u_M(x) - D^\mu u_M(x) - u_M(px) - D^\delta u_M(px) - f(x) = Res, \tag{20}$$

where *Res* is the residue function. By using equations (19) and (20), we have

$$\begin{aligned} D^{\beta}(u_M(x)-u(x))-(u_M(x)-u(x)) \quad &- \quad D^{\mu}(u_M(x)-u(x))-(u_M(px)-u(px)) \\ &- \quad D^{\delta}(u_M(px)-u(px))=Res. \end{aligned} \tag{21}$$

Let $\epsilon_M(x)=u_M(x)-u(x)$, then from equation (21) we get

$$D^{\beta}\epsilon_M(x)-\epsilon_M(x)-D^{\mu}\epsilon_M(x)-\epsilon_M(px)-D^{\delta}\epsilon_M(px)=Res. \tag{22}$$

with the initial conditions;

$$\epsilon^{(n)}(0)=0,\ n=\{0,1,\dots\lceil\beta\rceil-1\}.$$

Define the residual

$$\mathrm{Res}(x):=D^{\beta}u_M(x)-u_M(x)-D^{\mu}u_M(x)-u_M(px)-D^{\delta}u_M(px)-f(x).$$

Subtracting (19) from (20) yields the error equation (22) for $\epsilon_M(x):=u_M(x)-u(x)$ with zero initial data. Applying J^{β} to (22) and using the operational matrices of Section 3 gives

$$\epsilon_M(x)=P_{(x,\beta)}\epsilon_M(x)+P_{(x,\beta-\mu)}\epsilon_M(x)+P_{(px,\beta)}\epsilon_M(px)+P_{(px,\beta-\delta)}\epsilon_M(px)+J^{\beta}\mathrm{Res}(x).$$

Collocation at the nodes $\{x_i\}_{i=0}^{M}$ leads to

$$(I-A)\,E=J_{\beta}\,R,$$

where E collects the Bell coefficients of ϵ_M, A is assembled from the same operational matrices as in Section 4, $R=[\mathrm{Res}(x_i)]$, and J_{β} is the sampled J^{β}. Hence

$$\|E\|\le\|(I-A)^{-1}\|\,\|J_{\beta}\|\,\|R\| \quad\Rightarrow\quad \|\epsilon_M\|_{\infty}\le C\,\|\mathrm{Res}\|_{\infty},$$

with a constant C depending only on β,μ,δ,p and the collocation matrix. Consequently, if $\|\mathrm{Res}\|_{\infty}=O(M^{-r})$ (resp. $O(\rho^{-M})$), then $\|\epsilon_M\|_{\infty}=O(M^{-r})$ (resp. $O(\rho^{-M})$).

6. Illustrative examples

In this section, we assess the efficiency and applicability of the proposed method (discussed in Section 4) by applying it to five illustrative examples. The reported results are systematically compared with exact solutions to the provided problems, along with results obtained from other methods documented in the existing literature.

All simulations were implemented in MATLAB R2021a using our own codes for the proposed method. Linear systems were solved with `linsolve` (equivalent to the backslash operator and relying on LAPACK/BLAS). All runs were executed on a personal computer; the reported CPU and wall times are those returned by MATLAB.

6.1. Example 1

Consider the fractional-order pantograph differential equation [29]:

$$D^{\beta}u(x)=u(x)+\frac{1}{10}u\left(\frac{1}{10}x\right)+f(x), \tag{23}$$

with

$$u(0)=0$$

where

$$f(x) = \frac{2\beta}{\Gamma(3-\beta)}x^{2-\beta} - 1.1 - \beta x^2 - \frac{\beta}{1000}x^2$$

The exact solution is given by $u(x) = 1 + \beta x^2$.

By utilizing the operator of R–L fractional integral of order β on both sides of (23), we get

$$u(x) - u(0) = J^\beta u(x) + \frac{1}{10}J^\beta u\left(\frac{1}{10}x\right) + J^\beta f(x). \tag{24}$$

Now, approximating the $u(x)$ by using (10), and also using the given initial condition, we get

$$\mathbf{K}^T\mathbf{B}_{M,\gamma}(x) = J^\beta\left[\mathbf{K}^T\mathbf{B}_{M,\gamma}(x)\right] + \frac{1}{10}J^\beta\left[\mathbf{K}^T\mathbf{B}_{M,\gamma}\left(\frac{1}{10}x\right)\right] + J^\beta f(x). \tag{25}$$

As a next step, by using the equation (7) in (25), we get

$$\begin{aligned}\mathbf{K}^T[\mathbf{C}_M\mathbf{V}_{M,\gamma}(x)] &= \mathbf{K}^T[\mathbf{C}_M J^\beta(\mathbf{V}_{M,\gamma}(x))] \\ &+ \frac{1}{10}\mathbf{K}^T\left[\mathbf{C}_M J^\beta\left(\mathbf{V}_{M,\gamma}\left(\frac{1}{10}x\right)\right)\right] + J^\beta f(x).\end{aligned} \tag{26}$$

Now, by utilizing the generalized Bell operational matrix of fractional integration (12) in equation (26), we get

$$\begin{aligned}\mathbf{K}^T[\mathbf{C}_M\mathbf{V}_{M,\gamma}(x)] &= \mathbf{K}^T[\mathbf{C}_M\mathbf{P}_{(x,\beta)}\mathbf{V}_{M,\gamma}(x)] \\ &+ \frac{1}{10}\mathbf{K}^T\left[\mathbf{C}_M\mathbf{P}_{(\frac{1}{10}x,\beta)}\mathbf{V}_{M,\gamma}\left(\frac{1}{10}x\right)\right] + J^\beta f(x).\end{aligned} \tag{27}$$

For solving this problem, we choose $m = 4$ and determine the collocation points as the following:

$$\left\{x_0 = 0, x_1 = \frac{1}{4}, x_2 = \frac{2}{4}, x_3 = \frac{3}{4}, x_4 = 1\right\} \tag{28}$$

Using these collocation points in the equation (27), we get five algebraic equations with the vector of unknown coefficients $K^T = [k_0, k_1, k_2, k_3, k_4]$.

Solving the system of five algebraic equation for $\beta = 1$ by use of MATLAB software, we get the coefficient vector as the following:

$$\begin{aligned}K^T = [&1.0 \ -0.999999999999919 \ 0.999999999999870 \\ &0.000000000000057 \ -0.000000000000007]\end{aligned} \tag{29}$$

for the choose of $m = 4$.

As a final step, using the determined coefficients (29) in the equation (10), we get the approximate solution of the problem (23) in the following form:

$$\begin{aligned}u_M(x) &= 1 + 0.000000000000514x^\gamma + 0.999999999999992x^{2\gamma} \\ &+0.000000000000015x^{3\gamma} - 0.000000000000007x^{4\gamma}.\end{aligned} \tag{30}$$

Therefore, the function for error estimation becomes

$$\begin{aligned}\epsilon_M(x) &= 0.000000000000514x^\gamma - \beta x^2 + 0.999999999999992x^{2\gamma} \\ &+0.000000000000015x^{3\gamma} - 0.000000000000007x^{4\gamma}.\end{aligned} \tag{31}$$

In Table 1, we present the absolute errors for the values of $\beta = 0.25, 0.75, 1$ with $\gamma = 1$. The results are compared with the Modified Operational Matrix Method (MOMM) [29]. Analysis of the data in Table

Table 1: Comparative results for obtained absolute errors and CPU time from Example 1.

x	Present Method	MOMM	Present Method	MOMM	Present Method	MOMM
	$\beta = 0.25$	$\beta = 0.25$	$\beta = 0.75$	$\beta = 0.75$	$\beta = 1$	$\beta = 1$
0	0	0	0	0	0	0
0.2	4.44×10^{-16}	2.1×10^{-12}	0	2.2×10^{-12}	2.22×10^{-16}	1.0×10^{-15}
0.4	6.66×10^{-16}	2.3×10^{-12}	0	2.4×10^{-12}	4.44×10^{-16}	1.4×10^{-15}
0.6	1.11×10^{-15}	2.4×10^{-12}	2.22×10^{-16}	2.7×10^{-12}	2.22×10^{-16}	1.9×10^{-15}
0.8	1.99×10^{-15}	2.6×10^{-12}	0	2.9×10^{-12}	2.22×10^{-16}	2.1×10^{-15}
1	1.99×10^{-15}	2.9×10^{-12}	2.22×10^{-16}	3.0×10^{-12}	2.22×10^{-16}	2.3×10^{-15}
CPU time	0.002005s	-	0.000302s	-	0.002390s	-

1 unequivocally demonstrates that our proposed method delivers highly accurate approximations when contrasted with MOMM.

In Figures 1-4 (a), we visually showcase our results, providing a comparative analysis between exact and numerical solutions. Correspondingly, in Figures 1-4 (b), we depict the behavior of absolute errors for varying β values-specifically, $\beta = 1, 0.75, 0.5, 0.25$. These graphical representations underscore a remarkable agreement between exact and approximate solutions across different β values. Notably, the observed absolute error trends align with the chosen β values, illustrating a decrease in error as the β value approaches an integer.

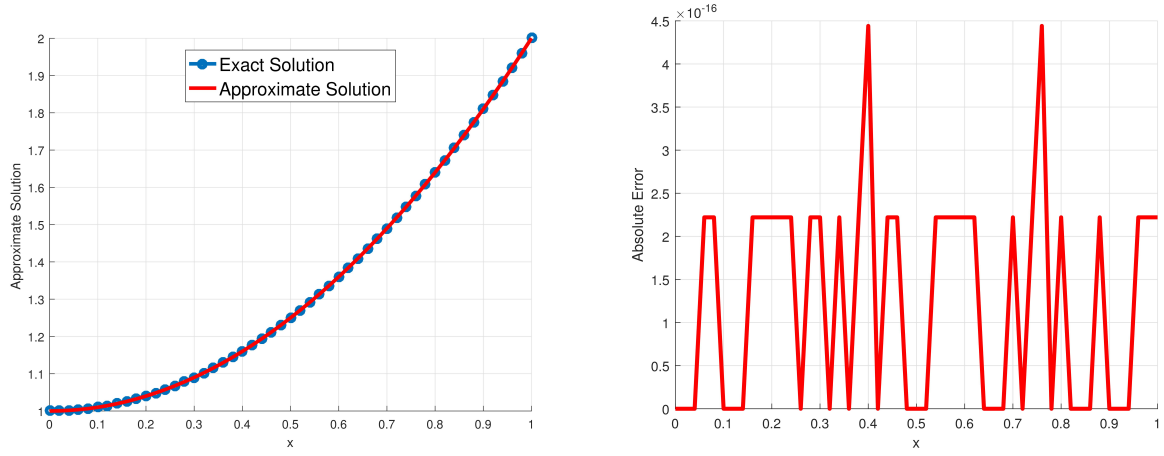

(a) (b)

Figure 1: **(a)** The comparison of exact and approximate solutions for the choice of $\beta = 1$. **(b)** The behaviour of absolute error for the choice of $\beta = 1$.

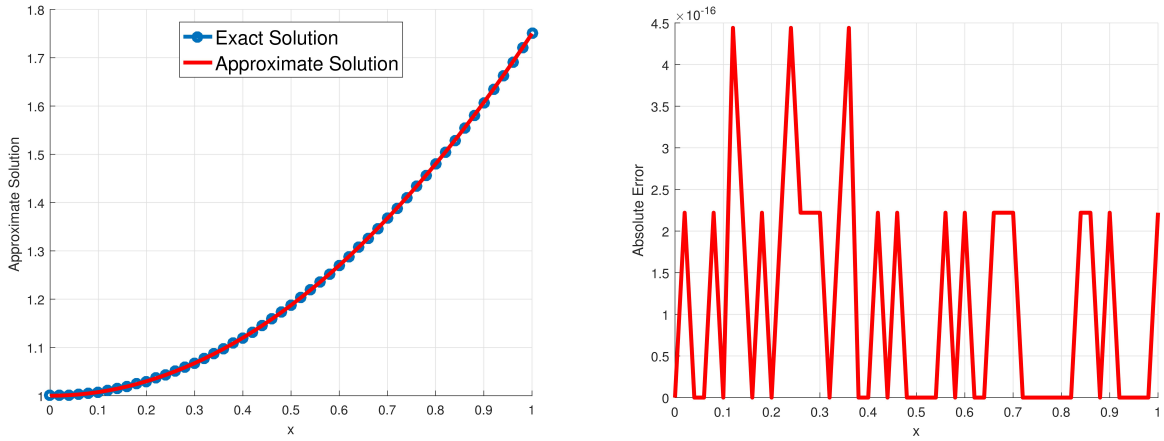

(a) (b)

Figure 2: **(a)** The comparison of exact and approximate solutions for the choice of $\beta = 0.75$. **(b)** The behaviour of absolute error for the choice of $\beta = 0.75$.

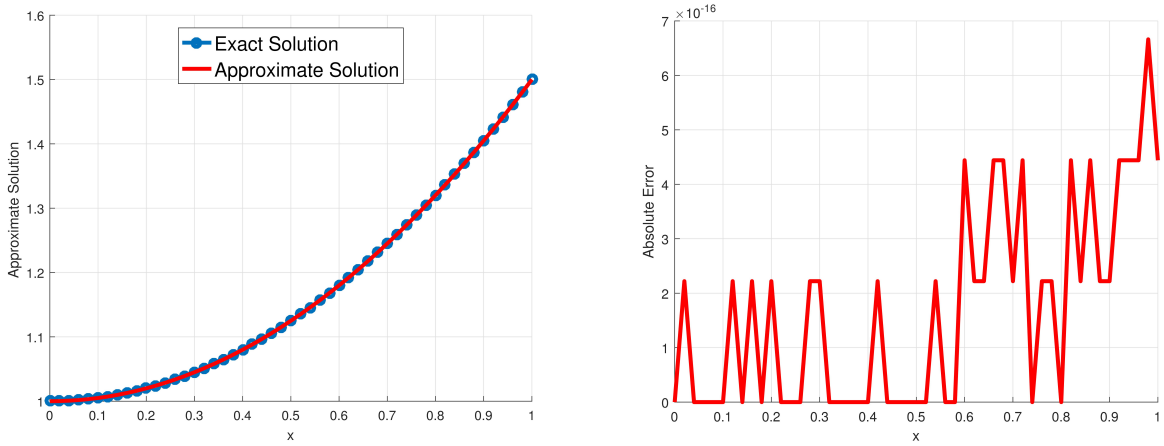

(a) (b)

Figure 3: **(a)** The comparison of exact and approximate solutions for the choice of $\beta = 0.5$. **(b)** The absolute error behaviour for the choice of $\beta = 0.5$.

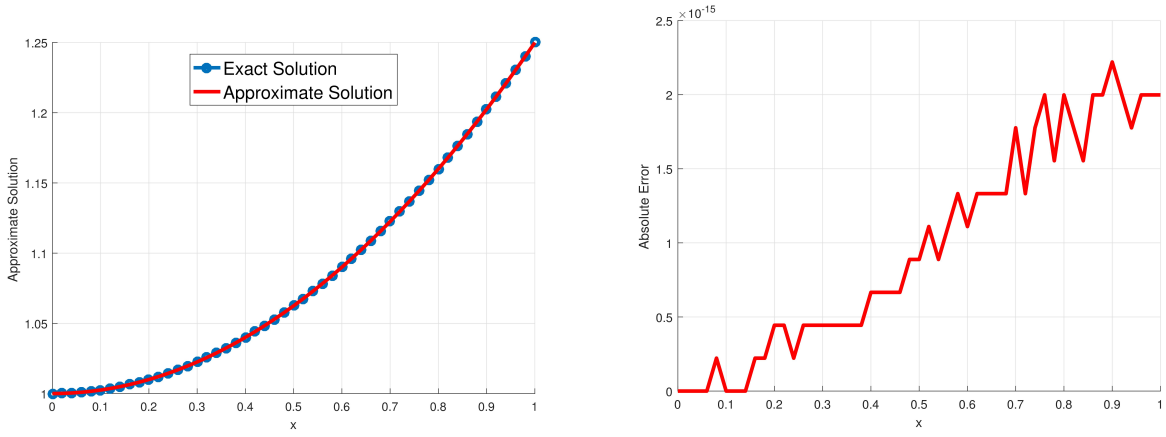

(a) (b)

Figure 4: **(a)** The comparison of exact and approximate solutions for the choice of $\beta = 0.25$. **(b)** The behaviour of absolute error for the choice of $\beta = 0.25$.

In Table 2, we give the comparisons between absolute and estimated errors for the choices of $\beta = 0.5, 0.75$, $\gamma = 1/2$ and $M = 10$. Also, the graphical demonstration of these comparisons are presented in Figures 5 (a) and (b) for $\beta = 0.5, 0.75$ respectively.

Table 2: Comparison of the absolute and estimated errors of Example 1 for choices of $\beta = 0.5, 0.75$ and $M = 10$.

x	Absolute error	Estimated error	Absolute error	Estimated error
	$\beta = 0.5$	$\beta = 0.5$	$\beta = 0.75$	$\beta = 0.75$
0.1	1.55×10^{-15}	3.94×10^{-15}	1.82×10^{-14}	1.10×10^{-14}
0.2	2.88×10^{-15}	1.68×10^{-15}	6.66×10^{-16}	1.81×10^{-14}
0.3	2.22×10^{-16}	6.28×10^{-16}	1.20×10^{-14}	1.55×10^{-14}
0.4	2.22×10^{-16}	4.69×10^{-15}	3.11×10^{-14}	6.03×10^{-15}
0.5	3.77×10^{-15}	1.01×10^{-14}	1.15×10^{-14}	1.47×10^{-14}
0.6	6.21×10^{-15}	1.58×10^{-14}	6.95×10^{-14}	5.08×10^{-14}
0.7	7.54×10^{-15}	1.92×10^{-14}	4.44×10^{-15}	1.89×10^{-14}
0.8	1.86×10^{-14}	2.96×10^{-14}	2.71×10^{-14}	6.75×10^{-14}
0.9	4.08×10^{-14}	4.39×10^{-14}	3.97×10^{-14}	4.55×10^{-15}
1	3.08×10^{-14}	4.79×10^{-14}	7.77×10^{-15}	4.87×10^{-14}

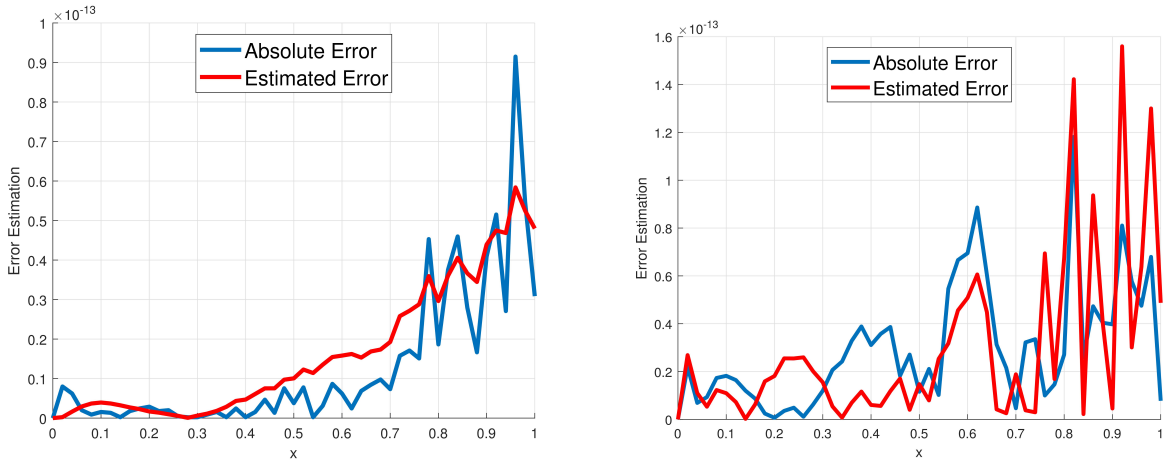

(a) $\beta = 0.5$ (b) $\beta = 0.75$

Figure 5: **(a)** Comparison of estimated and absolute errors for the choice of $\beta = 0.5$. **(b)** Comparison of estimated and absolute errors for the choice of $\beta = 0.75$

Upon examining the comparisons outlined in Table 2 and Figure 5, a notable alignment between the absolute and estimated error results becomes apparent. This consistency suggests that the error estimation method detailed in Theorem 3 can be effectively applied to problems where exact solutions are unavailable, thereby enhancing the efficiency of error estimation in such scenarios.

In Figure 6, we provide a graphical representation of absolute errors corresponding to various choices of β, with $\gamma = 1/2$. These visualizations reveal a consistent trend where the absolute error decreases as the order of the problem approaches an integer. This behavior aligns with the integer selection of the γ value. However, a noticeable increase in absolute error is observed when compared to the scenario where γ is an integer for the given problem (23).

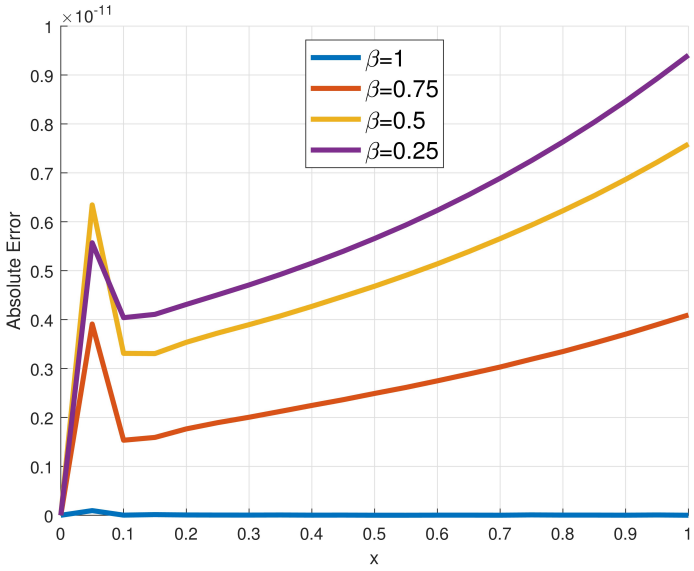

Figure 6: Absolute errors of Example 1 for $\gamma = 1/2$ and different choices of β.

6.2. Example 2

In this example, we focus on the solution of the fractional pantograph differential equation given as [32]:

$$D^{\beta}u(x) = -u(x) + \frac{1}{10}u\left(\frac{4}{5}x\right) + \frac{1}{2}D^{\beta}u\left(\frac{4}{5}x\right) + \left(\frac{8}{25}x - \frac{1}{2}\right)e^{-\frac{4}{5}x} + e^{-x}, \tag{32}$$

with

$$u(0) = 0,$$

and $\beta \in (0, 1]$ where $u(x) = xe^{-x}$ is the exact solution for $\beta = 1$.

In Table 3, we present the absolute errors derived from our method and contrast them with the absolute errors obtained using the Runge-Kutta [11], Bernoulli wavelet [23], and Legendre wavelet [32] methods. These comparisons clearly demonstrate the notable efficiency of our proposed technique relative to some established methods in the existing literature.

Table 3: Comparative results for absolute errors and CPU time in Example 2; the number of basis functions is set to $M = 6$ for all basis-based methods.

x	Present Method	Runge Kutta	Bernoulli wavelet	Legendre wavelet
0.1	4.85×10^{-14}	8.68×10^{-4}	1.98×10^{-8}	9.76×10^{-9}
0.3	3.02×10^{-14}	1.90×10^{-3}	7.78×10^{-9}	5.67×10^{-9}
0.5	2.69×10^{-14}	2.28×10^{-3}	6.34×10^{-5}	7.75×10^{-9}
0.7	3.71×10^{-14}	2.27×10^{-3}	4.36×10^{-5}	6.91×10^{-9}
0.9	3.92×10^{-14}	2.03×10^{-3}	2.80×10^{-5}	5.57×10^{-9}
CPU time	0.0020120s	-	-	-

In Figure 7 (a), the comparison of the exact and numerical solutions, and in Figure 7 (b) the behaviour of absolute errors for $\beta = 1$ are graphically demonstrated for the problem (32).

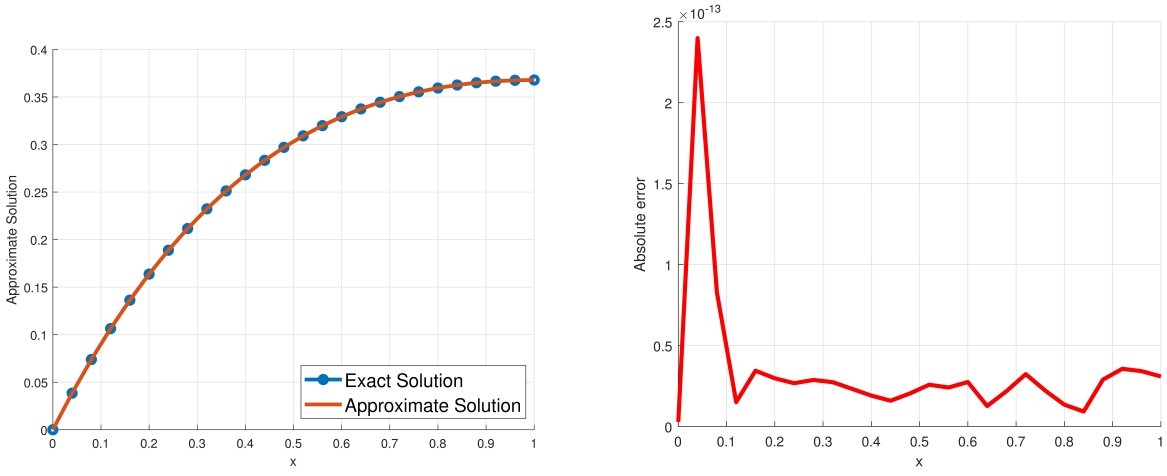

(a) (b)

Figure 7: **(a)** The comparison of exact and approximate solutions with the choice of $\beta = 1$. **(b)** The behaviour of absolute error for the choice of $\beta = 1$.

In Figure 8, we present a visual comparison between the numerical solutions generated by the introduced method for various choices of β and the exact solution of the given problem (32) within the interval $x \in [0, 15]$.

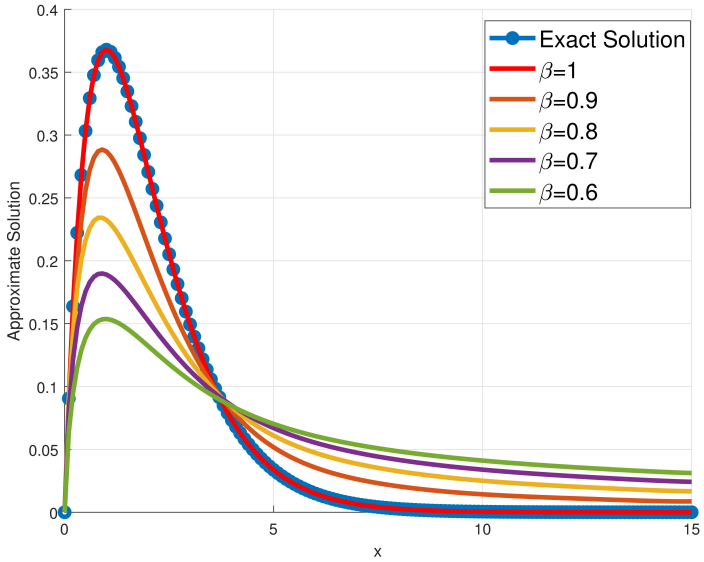

Figure 8: Approximate solutions of Example 2 for different choices of β when $x \in [0, 15]$.

6.3. Example 3

Consider the following fractional pantograph differential equation [26]:

$$D^{\beta}u(x) = \frac{3}{4}u(x) + u\left(\frac{x}{2}\right) + 2 - x^2, \tag{33}$$

with

$$u(0) = u'(0) = 0.$$

The exact solution of the problem is given by $u(x) = x^2$ for $\beta = 2$.

We address the specified problem (33) using our method with the parameters $M = 5$ and $\gamma = 1$. In Table 4, we present the absolute errors obtained from our method and compare them with the Chebyshev wavelet method (CWM) [16] and Chebyshev polynomials method (CPM) [26]. The results in the table unequivocally demonstrate the superior accuracy of our proposed method, even for a relatively small step size M, compared to both CWM and CPM methods.

In Figure 9 (a), the comparison of the exact and numerical solutions, and in Figure 7 (b) the behaviour of absolute errors for $\beta = 2$ are graphically demonstrated for the problem (33) where $x \in [0, 1]$.

Table 4: Comparative results for obtained absolute errors from Example 3.

x	Present Method	CWM	CPM
0.00	0	1.00×10^{-10}	4.21×10^{-15}
0.01	1.13×10^{-17}	1.00×10^{-10}	4.06×10^{-15}
0.02	1.42×10^{-17}	1.00×10^{-10}	3.81×10^{-15}
0.03	2.66×10^{-17}	1.00×10^{-10}	3.70×10^{-15}
0.04	3.08×10^{-17}	1.00×10^{-10}	3.56×10^{-15}
0.05	3.38×10^{-17}	1.00×10^{-10}	3.32×10^{-15}
0.06	1.95×10^{-17}	1.00×10^{-10}	3.19×10^{-15}
0.07	4.16×10^{-17}	1.00×10^{-10}	3.20×10^{-15}
0.08	3.30×10^{-17}	1.00×10^{-10}	3.11×10^{-15}
0.09	3.64×10^{-17}	1.00×10^{-10}	2.89×10^{-15}
0.10	4.51×10^{-17}	1.00×10^{-10}	2.74×10^{-15}

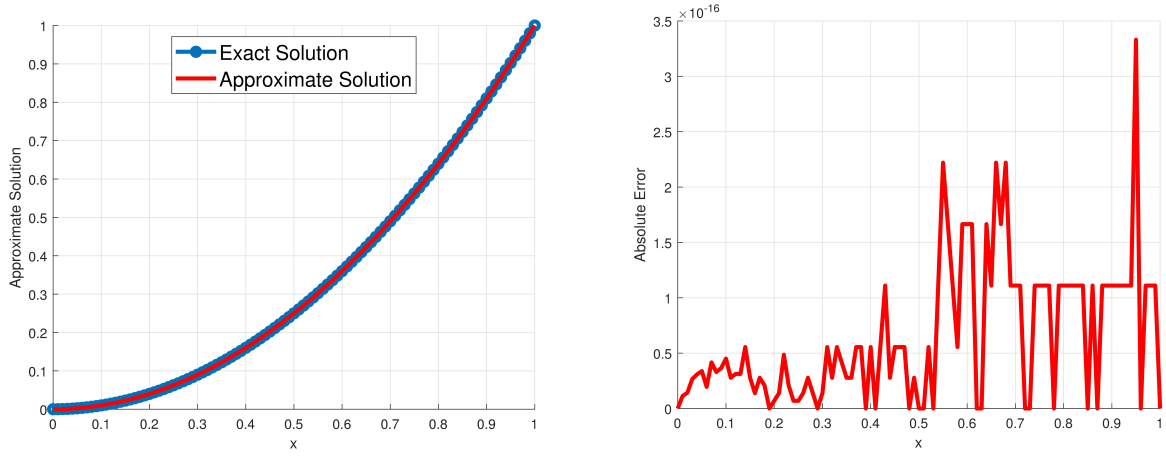

(a) (b)

Figure 9: **(a)** The comparison of exact and approximate solutions with the choice of $\beta = 2$. **(b)** The behaviour of absolute error for the choice of $\beta = 2$.

In Figure 10, numerical solutions of Example 3 computed by the proposed scheme for the various choices of β are compared with the exact solution of the given problem (33) where $x \in [0, 1]$.

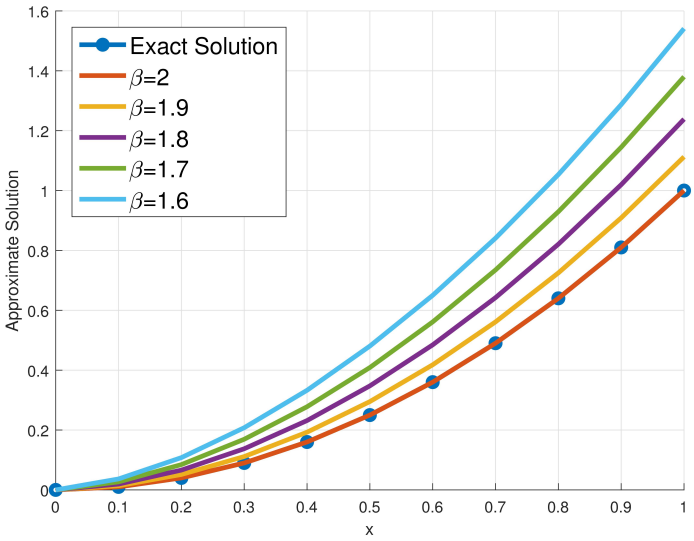

Figure 10: Comparison of the exact and approximate solutions for different choices of β.

6.4. Example 4

Consider the following type of linear fractional pantograph differential equation [15]:

$$D^{\frac{1}{2}}u(x) = -u(x) + \frac{1}{4}u\left(\frac{x}{3}\right) + \frac{1}{3}D^{\frac{1}{2}}u\left(\frac{x}{3}\right) + f(x), \quad x \in [0,1] \tag{34}$$

with

$$u(0) = 0.$$

where

$$f(x) = \frac{\Gamma(c+1)}{\Gamma(c+\frac{1}{2})}x^{c-\frac{1}{2}} + x^c - \frac{1}{4}\left(\frac{x}{3}\right)^c - \frac{1}{3}\frac{\Gamma(c+1)}{\Gamma(c+\frac{1}{2})}\left(\frac{x}{3}\right)^{c-\frac{1}{2}}$$

The exact solution is given by $u(x) = x^c$ for $c \geq \left\lceil \frac{1}{2} \right\rceil$.

We address the specified problem (34) utilizing our method with the parameters $\gamma = 1/2$ and $M = 10$. Table 5 presents the absolute errors obtained from our proposed method alongside the results reported from the shifted Gegenbauer-Gauss collocation (SGGCM) [15], considering choices of $c = 1, 1.5, 1.9$. These comparisons unequivocally highlight the superior performance of our method, showcasing better results across each choice of c and even for a smaller step size M when compared to SGGCM.

In Figure 11, the acquired approximate solution for the problem (34) using our method is graphically compared with the given exact solution for $c = 1$ where $x \in [0,1]$.

Table 5: Comparative results for obtained absolute errors and CPU time from Example 4.

x	Present Method	SGGCM	Present Method	SGGCM	Present Method	SGGCM
	$c = 1$	$c = 1$	$c = 1.5$	$c = 1.5$	$c = 1.9$	$c = 1.9$
0.1	1.71×10^{-17}	1.26×10^{-4}	4.39×10^{-13}	7.97×10^{-5}	2.57×10^{-7}	4.58×10^{-6}
0.2	2.78×10^{-17}	8.68×10^{-5}	1.02×10^{-13}	1.07×10^{-4}	4.56×10^{-8}	9.35×10^{-6}
0.3	1.91×10^{-17}	3.54×10^{-4}	6.66×10^{-15}	3.70×10^{-5}	4.52×10^{-9}	1.10×10^{-6}
0.4	5.55×10^{-17}	1.04×10^{-4}	1.84×10^{-14}	3.05×10^{-6}	2.04×10^{-8}	1.47×10^{-6}
0.5	0	3.99×10^{-4}	3.05×10^{-14}	5.44×10^{-5}	2.70×10^{-8}	5.96×10^{-6}
0.6	0	2.86×10^{-4}	3.56×10^{-14}	7.91×10^{-5}	2.96×10^{-8}	8.49×10^{-6}
0.7	4.89×10^{-17}	2.32×10^{-4}	3.75×10^{-14}	3.26×10^{-5}	3.02×10^{-8}	2.16×10^{-6}
0.8	1.11×10^{-16}	5.26×10^{-4}	4.23×10^{-14}	9.85×10^{-6}	2.96×10^{-8}	1.71×10^{-6}
0.9	3.29×10^{-16}	2.72×10^{-4}	4.05×10^{-14}	1.29×10^{-5}	2.86×10^{-8}	3.03×10^{-6}
1	2.22×10^{-16}	1.12×10^{-4}	3.88×10^{-17}	3.20×10^{-5}	2.73×10^{-8}	2.78×10^{-6}
CPU time	0.000112s	-	0.000230s	-	0.002791s	-

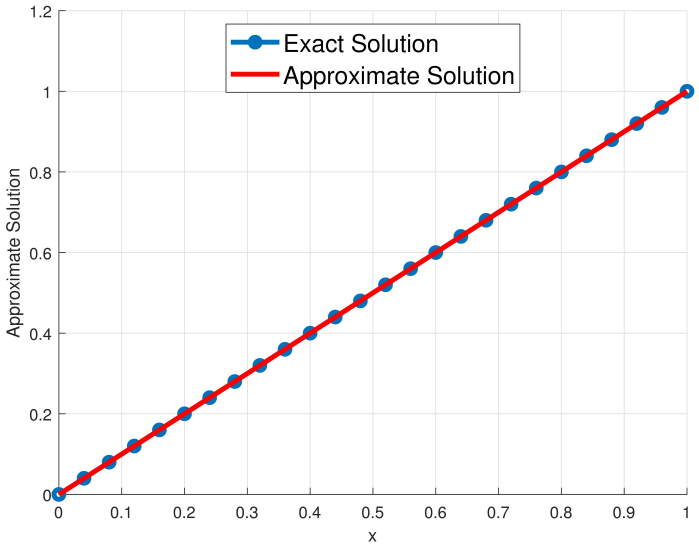

Figure 11: Comparisons for approximate and the exact solutions when $c = 1$ for Example 4.

In Figures 12-14 (a), we demonstrate behaviour of absolute errors for $\gamma = 1$, and in Figures 12-14 (b) we present the behaviour of absolute errors for $\gamma = 1/2$, for the choices of $c = 1, 1.5, 1.9$ respectively. When we compare the acquired absolute errors for the choices of $\gamma = 1$ and $\gamma = 1/2$, we can observe that, if we choose $\gamma = 1/2$, the proposed method reports better results for the problem (34) for the non-integer powers of the exact solution.

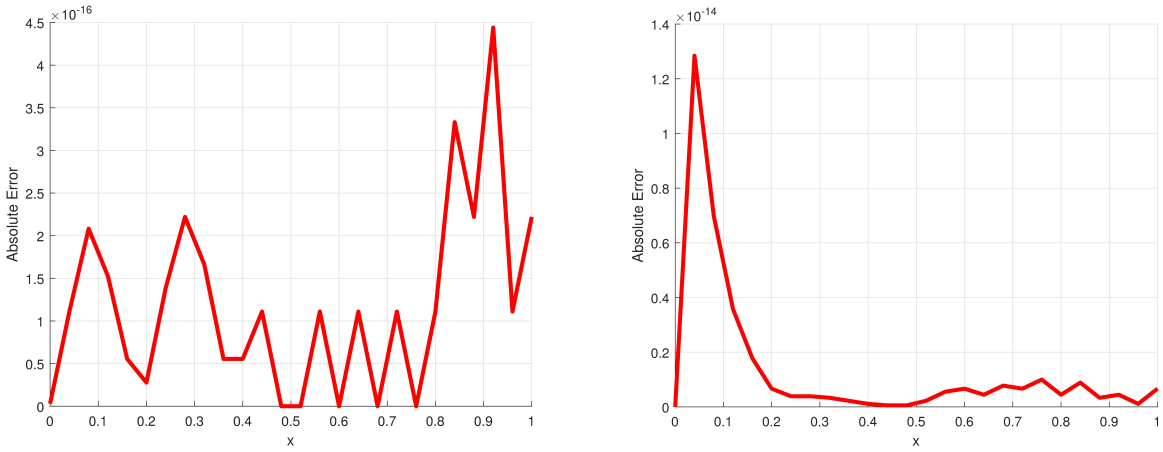

(a) $\gamma = 1$ (b) $\gamma = 1/2$

Figure 12: The graphical results for integer and non-integer values of γ when $c = 1$ for Example 4.

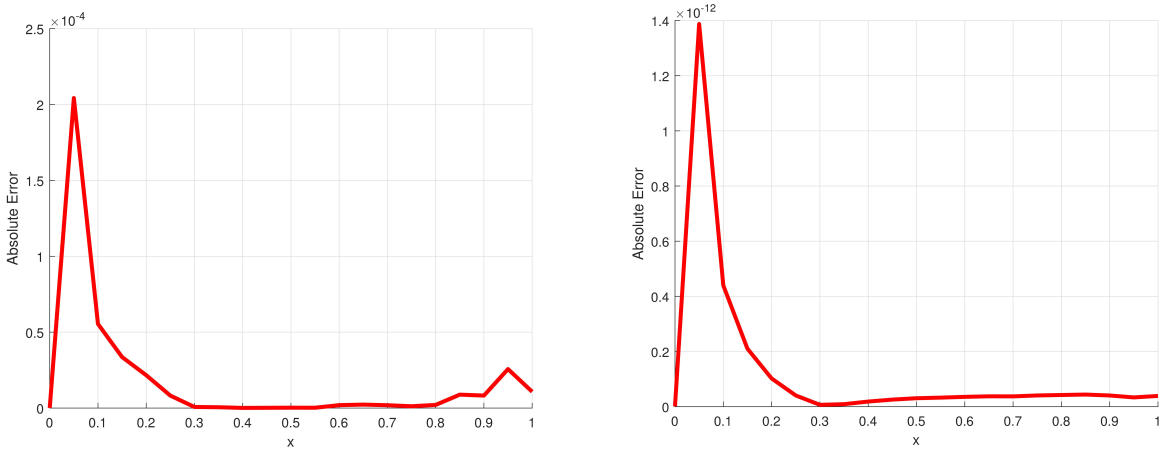

(a) $\gamma = 1$ (b) $\gamma = 1/2$

Figure 13: The graphical results for integer and non-integer values of γ when $c = 1.5$ for Example 4.

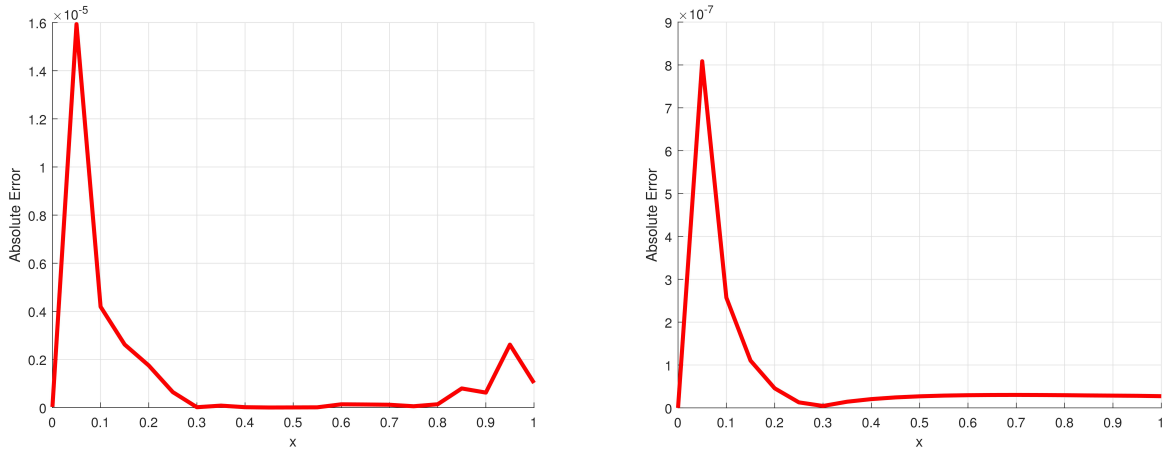

(a) $\gamma = 1$ (b) $\gamma = 1/2$

Figure 14: The graphical results for integer and non-integer values of γ when $c = 1.9$ for Example 4.

6.5. Example 5

As a last example, we consider on the fractional pantograph differential equation with multiple proportional delay[6]:

$$D^{\beta}u(x) = -\frac{5}{6}u(x) + 4u\left(\frac{x}{2}\right) + 9u\left(\frac{x}{3}\right) + x^2 - 1, \quad \beta \in (0, 1] \tag{35}$$

with

$$u(0) = 1.$$

The exact solution to this problem is given by $u(x) = 1 + \frac{67}{6}x + \frac{1675}{72}x^2 + \frac{12157}{1296}x^3$ for $\beta = 1$.

We solve the given problem (35) by use of proposed method with the selections of $M = 3$ and $\gamma = 1$. In Table 6, we present the exact and approximate solutions together with absolute errors computed by our method for the problem (35). From these presentations, it is very clear that the reported results by our method are in a high agreement with the actual solutions of the given problem. In Figures 15 (a) and (b), we illustrate the presented results in Table 6 graphically.

Table 6: Comparison of the exact and approximate solutions and produced absolute errors for Example 5.

x	Exact solutions	Approximate solutions	Absolute errors
0	1	1	0
0.1	2.35868595679012349	2.35868595679012394	4.44×10^{-16}
0.2	4.23893209876543331	4.23893209876543331	0
0.3	6.69702083333333320	6.69702083333333409	8.88×10^{-16}
0.4	9.78923456790123581	9.78923456790123936	3.55×10^{-15}
0.5	13.57185570987654266	13.57185570987654977	7.11×10^{-15}
0.6	18.10116666666666418	18.10116666666667840	1.42×10^{-14}
0.7	23.43344984567901790	23.43344984567902500	7.11×10^{-15}
0.8	29.62498765432099290	29.62498765432100356	1.07×10^{-14}
0.9	36.73206249999999784	36.73206250000001916	2.13×10^{-14}
1	44.81095679012345556	44.81095679012346267	7.11×10^{-15}

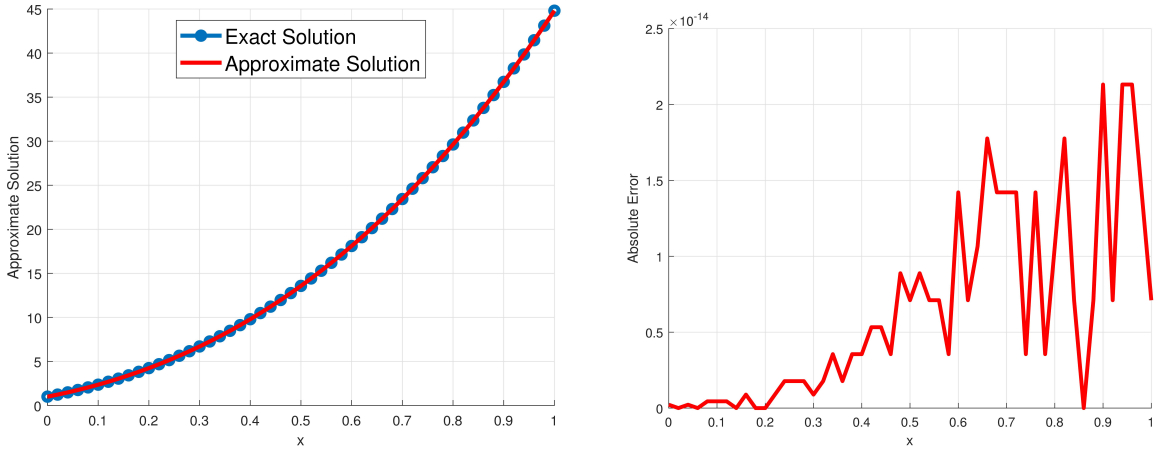

(a) (b)

Figure 15: **(a)** The comparison of exact and numerical solutions for the choice of $\beta = 1$. **(b)** The behaviour of absolute error for the choice of $\beta = 1$.

In Figure (16) (a), we illustrate the behavior of approximate solutions computed by the proposed method for the various choices of β together with the exact solution of the given problem (35) where $x \in [0, 1]$. And Figure (16) (b) demonstrates the same results for the case when $x \in [0, 5]$.

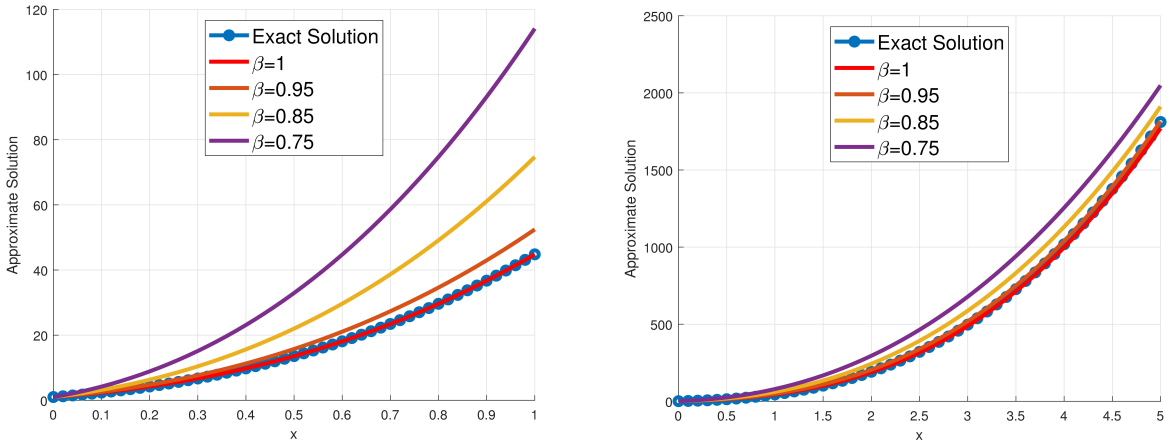

(a) (b)

Figure 16: **(a)** The comparison of exact and approximate solutions for various choices of β when $x \in [0, 1]$. **(b)** The comparison of exact and approximate solutions for various choices of β when $x \in [0, 5]$.

In Table 7, we present the obtained values for both absolute and estimated errors concerning the problem (35) with $\beta = 0.75$ and $\beta = 0.95$. Correspondingly, Figures 17 (a) and (b) visually depict these reported results for $\beta = 0.75$ and $\beta = 0.95$, respectively. The clear correspondence between the behaviors of absolute and estimated errors is evident from these findings, reinforcing the reliability and accuracy of the error estimation in our method.

Table 7: Comparative results for absolute and estimated errors from Example 5 with the choices of $\beta = 0.75, 0.95$.

x	Absolute Error	Estimated Error	Absolute Error	Estimated Error
	$\beta = 0.75$	$\beta = 0.75$	$\beta = 0.95$	$\beta = 0.95$
0	0	0	0	0
0.2	4.639	4.161	0.545	0.495
0.4	13.332	13.517	1.511	1.391
0.6	26.635	27.254	2.968	2.898
0.8	45.104	44.991	4.988	5.018
1	69.297	66.481	7.643	7.943

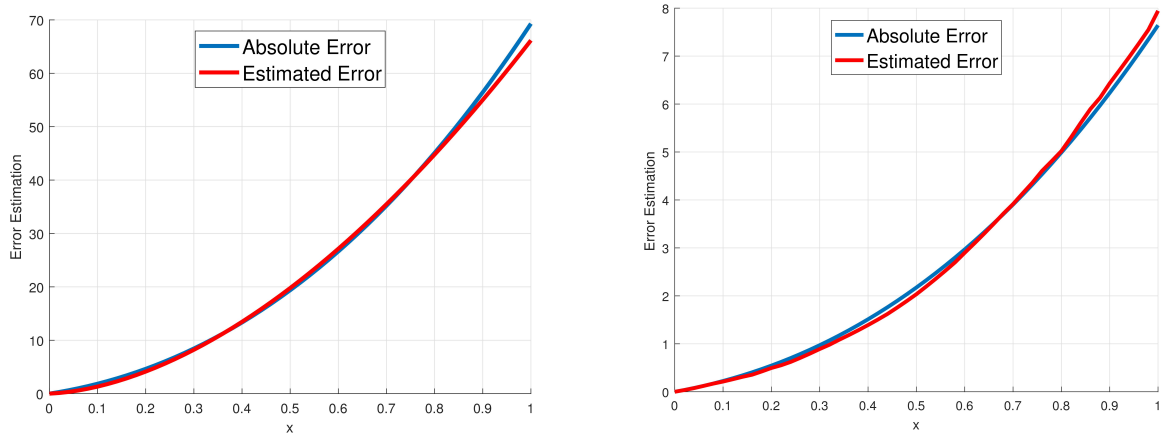

(a) $\beta = 0.75$ (b) $\beta = 0.95$

Figure 17: Absolute and estimated error comparison results for the Example 5.

6.6. Example 6

Consider the fractional nonlinear pantograph differential equation

$$\begin{cases} D^{\beta}u(x) = 1 - 2\left(u(\frac{x}{2})\right)^2, \quad 0 \le x \le 1,\ 1 < \beta \le 2, \\ u(0) = 1, \quad u'(0) = 0, \end{cases} \tag{36}$$

which involves a delayed nonlinear term $\left(u(x/2)\right)^2$.

Applying the proposed method, the solution is approximated as

$$u(x) \simeq K^T B_{M,\gamma}(x),$$

and the nonlinear delayed term is represented using the product operational matrix $Q^{(px,2)}$:

$$\left(u(\tfrac{x}{2})\right)^2 \simeq K^T Q^{(px,2)} B_{M,\gamma}(x).$$

Substituting into the integral form of (36) and collocating at the nodes $x_i = \frac{i}{M}T$ $(i = 0, 1, \ldots, M)$, we obtain a nonlinear algebraic system in K. This system is solved iteratively, and the approximate solution $u_*(t)$ follows.

For the integer case $\beta = 2$, the exact solution is $u(x) = \cos(x)$, which verifies the accuracy of the method.

Figure 18a compares the exact and numerical solutions for $\beta \in \{2.00, 1.90, 1.80, 1.70\}$; the curves are nearly indistinguishable, and the inset around $x \approx 0.7$ highlights only a minute discrepancy. In particular, for the benchmark case $\beta = 2.00$ the numerical solution virtually overlaps the exact solution, confirming the correctness of the implementation. Figure 18b reports the absolute error for $\beta = 2.00$ along $[0, 1]$, which remains at the level of machine precision (on the order of 10^{-12}), demonstrating the high accuracy and stability of the generalized Bell operational-matrix approach.

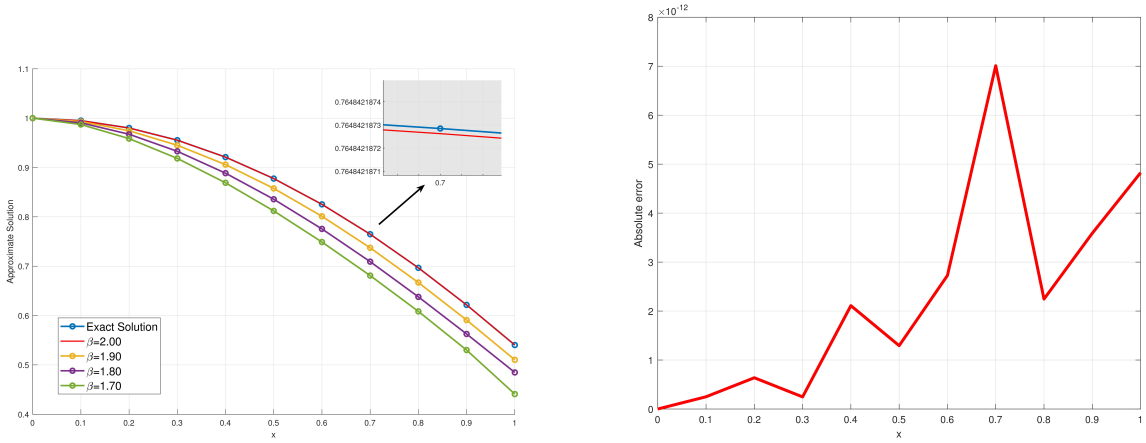

(a) (b)

Figure 18: (a) Comparison of exact and approximate solutions across fractional orders β; (b) absolute error at $\beta = 2.00$.

Table 8 reports the absolute errors at selected nodes for truncation levels $M \in \{3, 7, 9\}$, comparing the proposed generalized Bell operational–matrix method with the Bernoulli–wavelet scheme [23]. As M increases, the error of the proposed method decreases rapidly—reaching the 10^{-12}–10^{-13} range for $M = 9$—which is consistent with spectral–type convergence. Across the reported nodes, the proposed method is uniformly more accurate for $M = 3$ and $M = 9$, and remains competitive for $M = 7$ while avoiding the large local spikes observed for the Bernoulli–wavelet results (notably near $x \approx 0.6$–0.8). The bottom rows list CPU and wall times for the proposed method, indicating that the high accuracy is achieved with modest computational cost.

Figures 19(a)–(c) display the estimated error which is proposed in the Section 5.3 for $M = 3, 7, 9$, while Table 8 reports the corresponding absolute errors at the sampled nodes. The peak levels of the residual curves decrease steadily as M increases, and the error profiles remain smooth and bounded—exactly the same trend observed in Table 8, where the pointwise absolute errors shrink significantly from $M = 3$ to $M = 9$. The close agreement in magnitude and decay between the residual-based estimate and the true absolute error demonstrates that estimated is a reliable indicator of accuracy. Hence, even when an analytical solution is unavailable, the estimated error provides a meaningful and practical measure of the performance of the proposed method.

Table 8: Absolute error comparison between the proposed generalized Bell operational-matrix method and the Bernoulli wavelet method [23] for $M = 3, 7, 9$. CPU and wall times are reported for the proposed method.

	$M = 3$		$M = 7$		$M = 9$	
x	Present	Bernoulli	Present	Bernoulli	Present	Bernoulli
0.0	0	2.23×10^{-4}	0	1.05×10^{-10}	0	1.62×10^{-11}
0.2	3.543×10^{-4}	8.78×10^{-5}	6.678×10^{-10}	3.21×10^{-11}	6.380×10^{-13}	3.30×10^{-13}
0.4	2.731×10^{-4}	1.01×10^{-4}	4.101×10^{-10}	3.81×10^{-11}	2.111×10^{-12}	4.17×10^{-12}
0.6	4.136×10^{-4}	3.43×10^{-3}	8.279×10^{-10}	1.31×10^{-6}	2.727×10^{-12}	1.08×10^{-8}
0.8	6.216×10^{-5}	4.42×10^{-3}	1.492×10^{-9}	1.82×10^{-6}	2.245×10^{-12}	1.62×10^{-8}
CPU time	0.002500s	-	0.015625s	-	0.031250s	-
wall time	0.000904s	-	0.058520s	-	0.060649s	-

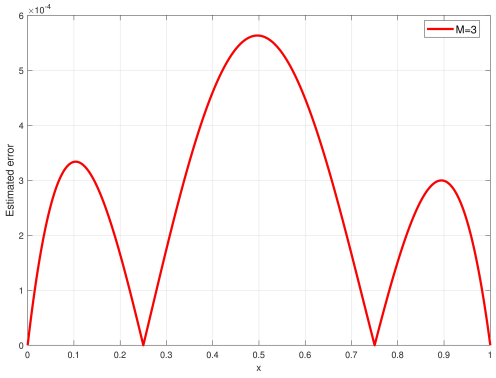

(a) Estimated error for $M = 3$.

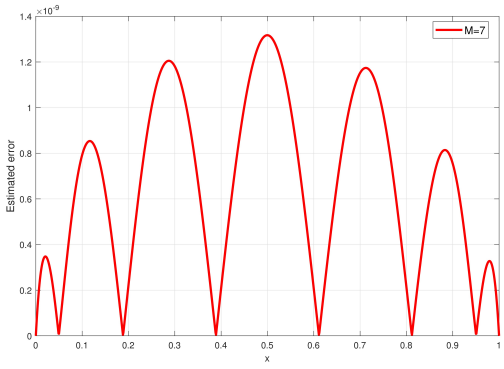

(b) Estimated error for $M = 7$.

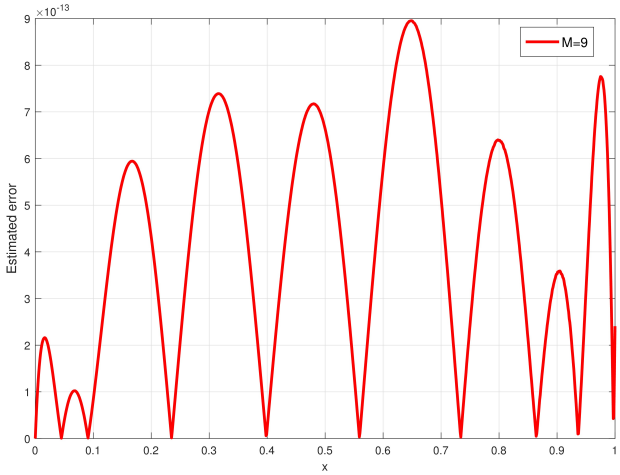

(c) Estimated error for $M = 9$.

Figure 19: Estimated errors for the Example 6.

6.7. Example 7

Consider

$$D^{1.2}u(x) = u^2(0.5x) + u^4(x) + g(x), \qquad x \in [0,1], \qquad u(0) = 0,\ u(1) = 1,$$

with

$$g(x) = \frac{\Gamma(2.8)}{\Gamma(1.6)}\, x^{0.6} - x^{7.2} - (0.5x)^{3.6},$$

whose exact solution is $u(x) = x^{1.8}$.

For choosing γ, we use the following rule of thumb provided in the Section 4: Near $x = 0$ the right–hand side is dominated by the term $x^{0.6}$ in $g(x)$; the delayed and nonlinear parts are of higher order when $u \sim x^r$. Thus $q = 0.6$ and, with $\alpha = 1.2$, the leading solution exponent is $r = \alpha + q = 1.8$. We choose $n = 2$ and set $\gamma_0 = r/2 = 0.9$; a short refinement scan around γ_0 confirms the minimum error near $\gamma \approx 0.90$, which we adopt. In the computations below we use $M = 8$.

Figures 20(a)–(b) report the results with the optimized choice $\gamma = 0.9$: the Bell approximation is visually indistinguishable from the exact solution and the absolute error remains uniformly small across $[0, 1]$. To illustrate the role of γ, we also show the outcome for $\gamma = 1$ in Figures 21(a)–(b). While the solution curve is still close to the exact profile, the absolute error is noticeably larger and exhibits oscillatory behaviour, highlighting the performance gain obtained by selecting γ via the proposed rule, with $\gamma = 0.9$ delivering the best accuracy for this example.

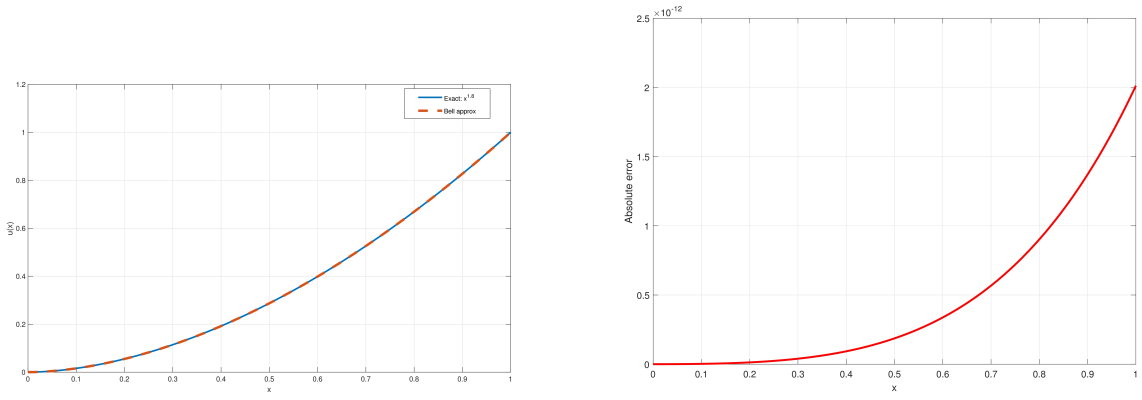

(a) (b)

Figure 20: (a) Comparison of exact and approximate solutions; (b) absolute error at $\gamma = 0.9$.

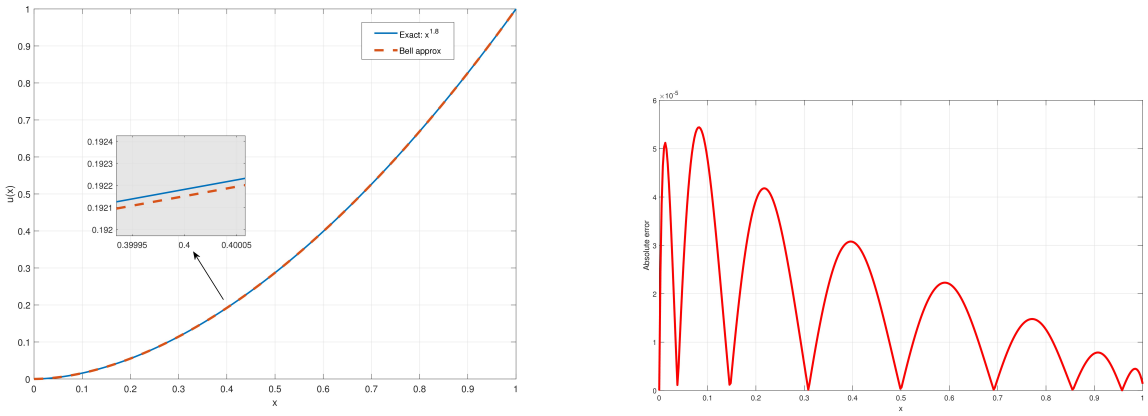

(a) (b)

Figure 21: (a) Comparison of exact and approximate solutions; (b) absolute error at $\gamma = 1$.

7. Conclusion and further research

In this study, we introduced an efficient numerical methodology based on generalized Bell polynomials for the resolution of multi-term fractional pantograph-type differential equations (FPDEs), including both linear and nonlinear forms. The core idea is to construct an operational matrix of fractional integration tailored to the generalized Bell basis vector and, when needed, employ projection-based matrices for nonlinear terms; this reduces the FPDE to a compact system of algebraic equations in the Bell coefficients. Given the difficulty of closed-form solutions for FPDEs, the proposed scheme provides practical and accurate approximations. Its applicability and effectiveness are confirmed through several illustrative examples and comparisons with existing methods, showing high accuracy with modest truncation levels and consistently low CPU times on a personal computer.

Looking ahead, beyond the nonlinear cases treated here, the approach can be further developed to address problems with variable-order operators and multiple delays, and to incorporate adaptive choices of the Bell parameter and refinement strategies, thereby broadening its scope in practical modeling scenarios.

References

[1] M. A. Abdelkawy and S. A. Alyami, *Legendre–Chebyshev spectral collocation method for two-dimensional nonlinear reaction–diffusion equation with Riesz space-fractional*, Chaos Solitons Fractals **151** (2021), 111279.
[2] I. Ahmad, R. Amin, T. Abdeljawad and K. Shah, *A numerical method for fractional pantograph delay integro-differential equations on Haar wavelet*, Int. J. Appl. Comput. Math. **7** (2021), 1–13.
[3] A. Akgül and S. A. Khoshnaw, *Application of fractional derivative on nonlinear biochemical reaction models*, Int. J. Intell. Netw. **1** (2020), 52–58.
[4] N. Ali, M. W. S. Khan and M. Sajid, *The Graetz–Nusselt problem for the curved channel using spectral collocation method*, Phys. Scr. **96** (2021), 055204.
[5] M. M. Alsuyuti, E. H. Doha, S. S. Ezz-Eldien and I. K. Youssef, *Spectral Galerkin schemes for a class of multi-order fractional pantograph equations*, J. Comput. Appl. Math. **384** (2021), 113157.
[6] H. Azin, M. H. Heydari and F. Mohammadi, *Vieta–Fibonacci wavelets: Application in solving fractional pantograph equations*, Math. Methods Appl. Sci. **45** (2022), 411–422.
[7] İ. Avcı and N. I. Mahmudov, *Numerical solutions for multi-term fractional order differential equations with fractional Taylor operational matrix of fractional integration*, Mathematics **8** (2020), 96.
[8] İ. Avcı, *Numerical simulation of fractional delay differential equations using the operational matrix of fractional integration for fractional-order Taylor basis*, Fractal Fract. **6** (2022), 10.
[9] İ. Avcı, *Spectral collocation with generalized Laguerre operational matrix for numerical solutions of fractional electrical circuit models*, Math. Model. Numer. Simul. Appl. **4** (2024), 110–132.
[10] E. T. Bell, *Exponential polynomials*, Ann. Math. **35** (1934), 258–277.
[11] A. Bellen and M. Zennaro, *Numerical Methods for Delay Differential Equations*, Oxford Univ. Press, Oxford, 2013.

[12] K. Diethelm, *The Analysis of Fractional Differential Equations: An Application-Oriented Exposition Using Differential Operators of Caputo Type*, Springer, Berlin, 2010.
[13] N. Engheia, *On the role of fractional calculus in electromagnetic theory*, IEEE Antennas Propag. Mag. **39** (1997), 35–46.
[14] R. Gorenflo, F. Mainardi, E. Scalas and M. Raberto, *Fractional calculus and continuous-time finance III: The diffusion limit*, in *Mathematical Finance*, Trends Math., Birkhäuser, Basel, 2001.
[15] R. M. Hafez and Y. H. Youssri, *Shifted Gegenbauer–Gauss collocation method for solving fractional neutral functional-differential equations with proportional delays*, Kragujevac J. Math. **46** (2022), 2022.
[16] M. A. Iqbal, A. Ali and S. T. Mohyud-Din, *Chebyshev wavelets method for fractional delay differential equations*, Int. J. Mod. Appl. Phys. **4** (2013), 49–61.
[17] V. V. Kulish and J. L. Lage, *Application of fractional calculus to fluid mechanics*, J. Fluids Eng. **124** (2002), 803–806.
[18] C. Lanczos, *Trigonometric interpolation of empirical and analytical functions*, J. Math. Phys. **17** (1938), 123–199.
[19] J. T. Machado, V. Kiryakova and F. Mainardi, *Recent history of fractional calculus*, Commun. Nonlinear Sci. Numer. Simul. **16** (2011), 1140–1153.
[20] R. L. Magin, *Fractional calculus models of complex dynamics in biological tissues*, Comput. Math. Appl. **59** (2010), 1586–1593.
[21] Z. M. Odibat and N. T. Shawagfeh, *Generalized Taylor's formula*, Appl. Math. Comput. **186** (2007), 286–293.
[22] M. D. Ortigueira and J. T. Machado, *Fractional calculus applications in signals and systems*, Signal Process. **86** (2006), 2503–2504.
[23] P. Rahimkhani, Y. Ordokhani and E. Babolian, *Numerical solution of fractional pantograph differential equations using generalized fractional-order Bernoulli wavelets*, J. Comput. Appl. Math. **309** (2017), 493–510.
[24] B. Ross, *A brief history and exposition of the fundamental theory of fractional calculus*, in *Fractional Calculus and Its Applications*, Springer, Berlin, 1975, pp. 1–36.
[25] M. Samraiz, Z. Perveen, T. Abdeljawad, S. Iqbal and S. Naheed, *On certain fractional calculus operators and applications in mathematical physics*, Phys. Scr. **95** (2020), 115210.
[26] H. Singh, *Numerical simulation for fractional delay differential equations*, Int. J. Dyn. Control **9** (2021), 463–474.
[27] H. Sun, Y. Zhang, D. Baleanu, W. Chen and Y. Chen, *A new collection of real-world applications of fractional calculus in science and engineering*, Commun. Nonlinear Sci. Numer. Simul. **64** (2018), 213–231.
[28] N. H. Sweilam, A. A. E. El-Sayed and S. Boulaaras, *Fractional-order advection–dispersion problem solution via the spectral collocation method and the nonstandard finite difference technique*, Chaos Solitons Fractals **144** (2021), 110736.
[29] M. I. Syam, M. Sharadga and I. Hashim, *A numerical method for solving fractional delay differential equations based on the operational matrix method*, Chaos Solitons Fractals **147** (2021), 110977.
[30] V. E. Tarasov and V. V. Tarasova, *Macroeconomic models with long dynamic memory: Fractional calculus approach*, Appl. Math. Comput. **338** (2018), 466–486.
[31] Y. H. Youssri, W. M. Abd-Elhameed, A. S. Mohamed and S. Sayed, *Generalized Lucas polynomial sequence treatment of fractional pantograph differential equation*, Int. J. Appl. Comput. Math. **7** (2021), 1–16.
[32] B. Yuttanan, M. Razzaghi and T. N. Vo, *Legendre wavelet method for fractional delay differential equations*, Appl. Numer. Math. **168** (2021), 127–142.
[33] Ş. Yüzbaşı, *A new Bell function approach to solve linear fractional differential equations*, Appl. Numer. Math. **174** (2022), 221–235.
[34] Ş. Yüzbaşı and G. Yıldırım, *A collocation method to solve the parabolic-type partial integro-differential equations via Pell–Lucas polynomials*, Appl. Math. Comput. **421** (2022), 126956.